Deciphering Immediate Post-Pulse Membrane Resealing from 4-Electrode Impedance Measurements by Numerical Modeling

Annabelle Collin, Tomás García-Sánchez, Sergio Corridore, Lluis Mir, Clair Poignard

Deciphering immediate post-pulse membrane resealing from 4–electrode impedance measurements by numerical modeling

Annabelle Collin*[1], Tomás García-Sánchez[2], Sergio Corridore[1], Lluis M. Mir[3], and Clair Poignard[1]

[1]Univ. Bordeaux, CNRS, INRIA, Bordeaux INP, IMB, UMR 5251, F–33400 Talence, France
[2]Department of Information and Communication Technologies, Universitat Pompeu Fabra, Barcelona, Spain
[3]METSY, UMR 9018, Université Paris-Saclay, CNRS, Gustave Roussy, 94805 Villejuif, France

Abstract

Background and Objective: The present paper proposes a numerical strategy to decipher the dynamics of the cell membranes exposed to an electroporating electric field from bioimpedance measurements. In particular we aim at discriminating between the increase of membrane conductivity due to electroporation from the increase of buffer conductivity due to ion exchange between buffer and cells.
Methods: We propose first a robust calibration procedure that enables to account for the complexity of the 4–electrode experimental set-up. Thanks to this robust calibration, we deduce the impedance of the sample from the measurements. Then we propose a simple electrical circuit model of the set-up, which is calibrated into two steps.
Results: First we estimate the model parameters before the electroporating electric field, in order to obtain the cell parameters. The dynamic of the membrane resistance after the pulses is then calibrated simultaneously with the increase of the buffer conductivity due to ions exchanges. Interestingly, our model and our calibration strategy enable us to capture the dynamics of the cell membranes within a few seconds after the pulse. For longer times, we explain how additional measurements of the buffer conductivity should be performed to track the dynamics of the membrane resealing more accurately.
Conclusions: The combination of the robust calibration with the well-designed equivalent circuit model enables us to capture the dynamics of ions exchange and membrane permeabilisation within the few seconds after the electric pulse.

Keywords: Electrical modeling of cells; Numerical Optimization; Electroporation ; Impedancemetry ; 4-electrode measurements

*Corresponding author: annabelle.collin@inria.fr

1 Introduction

Electroporation consists in applying pulsed electric fields of high intensity and short duration (typically several hundreds of volts per centimeter during one hundred microseconds) to cells in order to create defects in the cell membrane. Since the last two decades, the phenomenon has been widely studied both in vivo and in vitro experiments. Interestingly it has been shown that this method selectively affects cell membrane structures and its properties [23], leading to therapeutic innovations. In particular, reversible electroporation makes it possible to introduce non permeant molecules (cytotoxic drugs like bleomycin, DNA plasmids) into living cells, without a direct killing [15, 12, 7, 14] while for higher electric pulse intensity or duration, the cells in the targeted region die by a non-thermal mechanism so-called irreversible electroporation (IRE) [4].

Mir's group have shown that the cell membrane remains permeable several minutes after microsecond pulses, leading to a well-designed clinical protocol for electrochemotherapy [16, 13], and Pakhomov *et al.* have shown similar results on nanosecond pulses [18]. Mir's group has also shown the dual phenomenon of electroporation: a rapid pore formation that quickly reseals and a long-term alteration of the membrane permeability [3].

It is worth noting that despite a lot of experimental evidences of the increase of membrane permeability after electric pulses, there is still a lack of knowledge on the electrical properties of the membrane in the minutes after the pulse. Bioimpedancemetry seems to be the method of choice to track such changes, thanks to the huge number of measures that can be performed. However it faces the difficult problem of electrode-solute interactions, that perturb the measures and their interpretations. Indeed, when an electrode is immersed in a solute with ions, a boundary layer around the electrode so-called Gouy-Chapman-Stern layer appears. In this layer the ion concentrations –thus the conductivity of the solute– are quite different from the concentrations in the bulk (far from the electrode). In other words, the electrode measurements are highly perturbed by this layer and the conductivity of the medium is hardly recovered accurately [11]. In addition, the thickness of the layer increases (nonlinearly) with the electric current injected to the electrode [20, 8]. Therefore a standard impedancemetry set-up applied to biological experiments leads to noisy and unusable results.

Schwan et al. proposed a 4-electrode experimental set-up to limit the size of the interface solute-electrode of measurements [21]. Roughly speaking, 2 electrodes deliver the current and 2 other, connected to a high input impedance, measure the potential. However the calibration of the system is far from trivial. Bao *et al.* proposed a well-designed set-up and the corresponding numerical method for calibration for the impedance spectroscopy of erythrocyte in [2]. Their calibration method is based on the impedance measurements of 3 samples whose electrical properties are known. The resolution of a nonlinear system enables then to determine the calibration functions. García-Sánchez *et al.* proposed a different 4–electrode experimental set-up, for which a specific calibration is required [6], as the method of Bao *et al.* leads to unstable calibration.

Usually, impedance measurements of cells in culture are performed using very dense cell suspensions to increase the ratio volume of the cells/volume of the buffer. By using attached cells, in a set-up that does not need to detach the cells (and that therefore respects the geometry and membrane characteristics of the cells), impedance measurements are performed in more physiological conditions. García-Sánchez *et al.* proposed recently such well-designed set-up. In particular, they proposed an experimental set-up for fast electrical impedance spectroscopy measurements (1 spectrum per millisecond) to study the evolution of the electrical properties of adherent cell myotubes within the milliseconds after the electroporating pulse [6].

The main goals of this paper is to present a robust calibration strategy of the 4-electrode experimental set-up of García-Sánchez *et al.* to investigate the electroporation of C2C12 my-

oblasts in buffers with different [KCl] concentrations based upon a well-designed equivalent electric circuit.

An optimization procedure to calibrate the experimental set-up is first proposed. It stabilises the calibration process of Bao *et al.*, which otherwise leads to inconsistent and unstable phase of the impedance. The second important result of the paper is the equivalent circuit model that enables us to account the changes of the cell electrical parameters before and after the pulses delivery. In particular our methodology combines robust calibration, circuit model and numerical optimization procedure. It enables us to discriminate between the exchange of ions before and after electroporation and the huge decrease of membrane resistivity. As a consequence, our third main result consists in discriminating between the postpulse exchange of ions between the cells and the buffer and the increase of membrane conductance due to permeabilization. Particularly, our calibration makes it possible to quantify the short-term behaviour –within a few seconds after the pulse– of the membrane conductance. We also propose in the discussion section an experimental strategy to track the long-lasting behaviour of the membrane, several minutes after the pulses.

2 Materials and Methods

2.1 Experimental set-up presentation

2.1.1 Device to perform electroporation and impedancemetry

The set-up proposed by García-Sánchez *et al.* consists of a disc of 15 mm diameter comprising six equally spaced micro-electrodes coiled in parallel around the center of the disc, see Figure 1-Top-Left. Each electrode is a spiral of almost five loops. It measures 75 μm of width and approximatively 10 cm long. The radial distance between two consecutive spirals is of 150 μm. The micro-electrodes device is placed on the top of the cell monolayer, avoiding direct contact to cells by means of microseparators, to deliver the electroporating pulses and to perform the impedancemetry (see Figure 1-Top-Right). Figure 1-Bottom shows a schematic section of the system.

The impedance measurement system is conceived to impose an AC voltage between electrodes $\mathcal{E}_1$ and $\mathcal{E}_2$. Then, the current flowing through the sample (I) is measured with a transimpedance amplifier.

The voltage difference between the inner electrodes $(E1-E2)$ & $(E3-E4)$ (V) is measured with a differential amplifier with the recording electrodes coupled two to two. This configuration with six electrodes leads to increase the measured area.

2.1.2 Buffers and cells

The buffer is initially composed of sucrose, Hepes and MgCl and its conductivity is measured to $\sigma_0 = 0.098$ S.m^{-1}. Then for the calibration the [KCl] concentration is increased by 25 mM from 0 mM to 100 mM to increase the buffer conductivity. For each concentration, an impedancemetry of the buffer is performed for the calibration of the experimental set-up.

After the culture of the C2C12 myoblasts into 24 multi-well plates seeded at an initial density of 15×10^3 cells per well, the buffer was added and the electrodes positioned. The direct contact between the electrodes and the cells is prevented by using microseparators of thickness 10 μm. Then the experiments are performed with 5 different [KCl] concentrations: $\{0, 5, 10, 20, 30\}$ mM. The cell monolayer is then submitted to one biphasic microsecond pulse (100 μs positive, followed by 10 μs delay and then 100 μs negative) at 12 V or 30 V corresponding

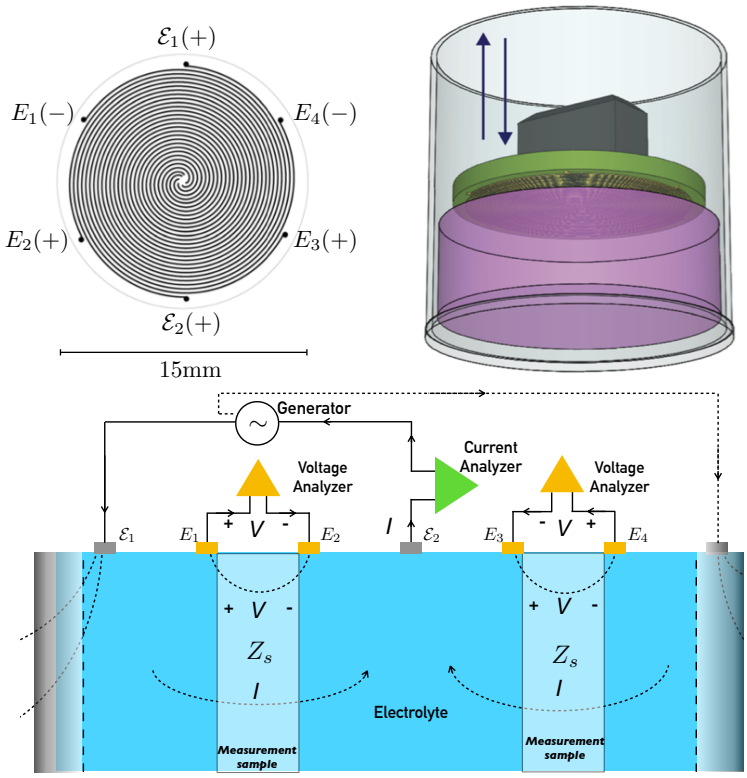

Figure 1: Top-Left: A representation of the spiral micro-electrode geometry. Two spirals correspond to the active electrodes ($\mathcal{E}_1$ and $\mathcal{E}_2$), and the other four spirals (E_1, E_2, E_3 and E_4) are used to measure the voltage. Top-Right: A representation of the experimental set-up. The micro-electrode is placed above the cells inside a cylindrical plate. Source: [6]. Bottom: 2D section of the arranged 4-electrode system. The sample under measure is the portion of buffer between the electrode measurement electrodes.

to a nominal electric field[1] of 800V/cm or 1200V/cm respectively.

2.2 Data presentation

2.2.1 Impedancemetry for the buffers

In order to calibrate the system, impedance measurements of the buffer alone (without the C2C12 myoblasts layer) are performed with 5 different [KCl] concentrations ranging from 0 mM to 100 mM at 26 frequencies ranging from 1 kHz to 1 MHz. Denote by F_{kHz} the set of the frequencies of measurements:

$$F_{\text{kHz}} = \{1, 3, 5, 7, 11, 15, 19, 25, 33, 41, 51, 63, 77, 95, 117, 143, 173, 209, \\ 253, 307, 371, 447, 539, 649, 781, 939\} \quad \text{in kHz},$$

and by C_{B} the set of the concentrations

$$C_{\text{B}} = \{0, 25, 50, 75, 100\} \quad \text{in mM}.$$

[1]The nominal electric field is the magnitude of the applied voltage divided by the distance between the active electrodes. It is not the electric field seen by the cell membrane.

The measured impedances of the buffers are denoted by

$$Z^{(\mathrm{c})}_{\mathrm{B},\mathcal{M}} : f \mapsto Z^{(\mathrm{c})}_{\mathrm{B},\mathcal{M}}(f), \qquad \forall (\mathrm{c}, f) \in C_{\mathrm{B}} \times F_{\mathrm{kHz}}.$$

Two sets of impedance measurements at frequencies in F_{kHz} are performed for each concentration. For each frequency, 1074 measurements are done. Figure 2 depicts the Bode plots. The continuous (experiment 1) or dotted (experiment 2) lines of Figure 2 correspond to the mean value of the 1074 measurements per frequency. At any frequency of F_{kHz}, for each curve, the error bar corresponds to 95% of the 1074 measures assuming that the measured impedances follow Gaussian distributions. In other words the error bars correspond to the interval

$$\left[Z^{(\mathrm{c})}_{\mathrm{B},\mathcal{M}}(f) - 1.96\,\sigma^{(\mathrm{c})}(f)\,, \quad Z^{(\mathrm{c})}_{\mathrm{B},\mathcal{M}}(f) + 1.96\,\sigma^{(\mathrm{c})}(f) \right].$$

Note that for each experiment, the variability among the 1074 measurements at any frequency is very small compared with the inter-experiments variability. Therefore, the variability comes from the experimental more than from the impedance meter, justifying the use of the mean value of the impedance.

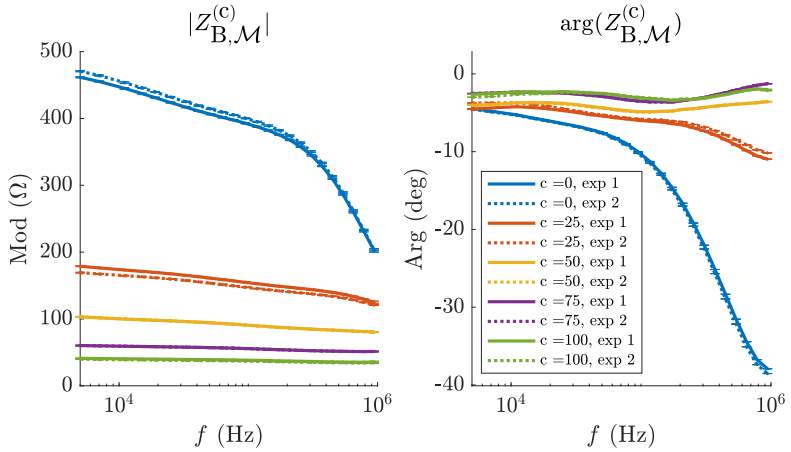

Figure 2: Bode plots of the impedances $Z^{(\mathrm{c})}_{\mathrm{B},\mathcal{M}}$ measured on 5 saline solutions with different [KCl] concentrations (in mM). For each continuous (resp. dotted) line, the error bars represent the 95% of the 1074 impedances measured at a given frequency for the first (resp. second) experiment.

2.2.2 Impedance measurements with cells

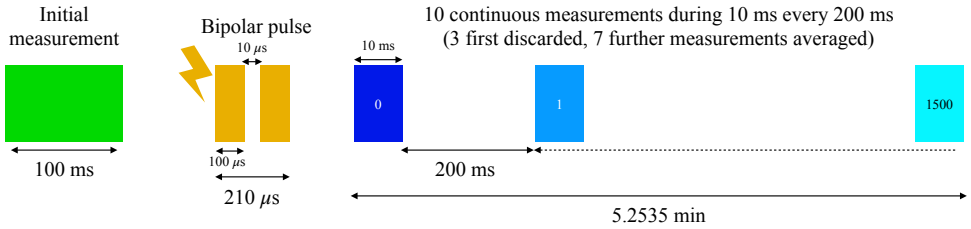

Figure 3: Scheme of the experiment.

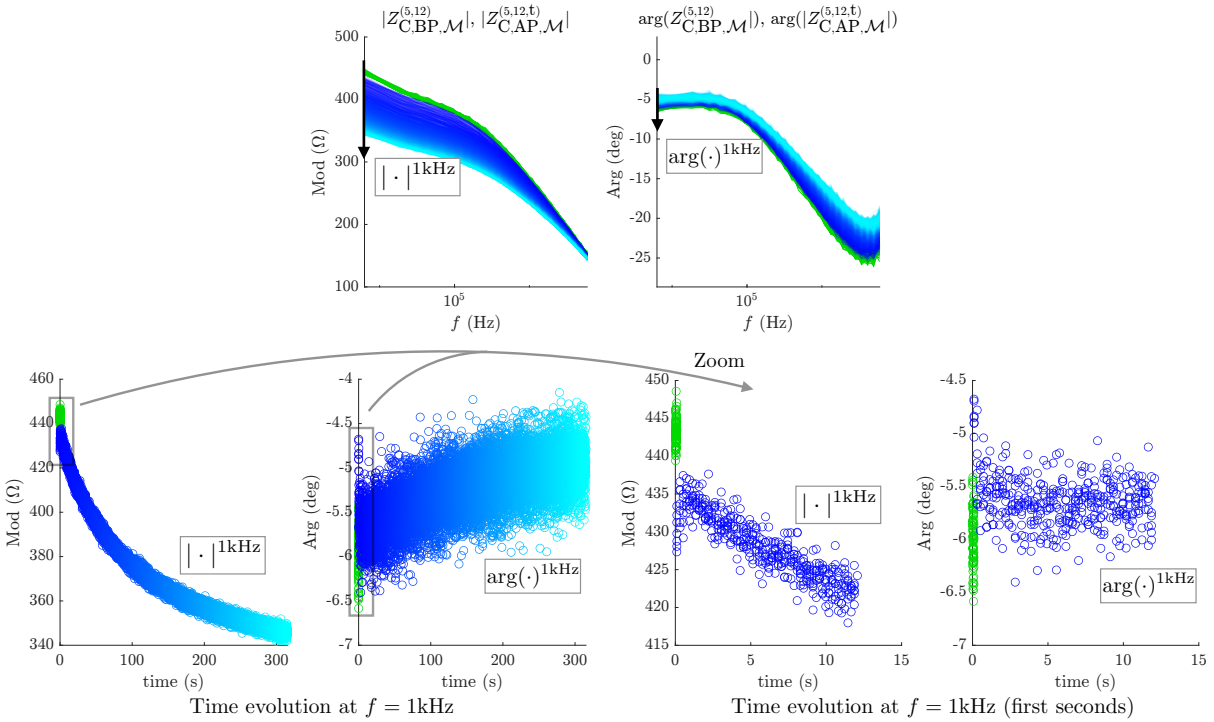

Figure 4: Top: Bode plots of the $Z^{(5,12)}_{C,BP,\mathcal{M}}$ and $Z^{(5,12,t)}_{C,AP,\mathcal{M}}$ (5 mM and 12 V). One can distinguish the measurements before the pulse (in green) and those done after the pulse during five minutes in blue – increasingly clear at the passage of the time, as explained by the scheme given in Figure 3. Bottom/Left: Corresponding time evolving curves for the frequency 1 kHz. Bottom/Right: Zoom on the beginning of the time evolving curves for the frequency 1 kHz.

First impedance measurements of buffer at different [KCl] concentration are performed, in order to calibrate the system. Then the impedance measurements of the different buffers with cell myoblasts are performed before and during the 5 minutes after the electroporation.

The measurement was initiated with 100 initial consecutive measurements (100 ms) pre-electroporation. Immediately the system was switched and one biphasic microsecond electroporating pulse was delivered at the corresponding voltage (12 or 30 V). After the pulse delivery, the system was switched back. Then, impedance was recorded every 200 ms for 10 ms with 10 consecutive measurements per point during approximately 5 minutes. One measurement lasts 1 ms. The 3 first measurements were discarded to avoid transients, and the 7 other measurements were averaged. This results in 1501 measurements. Here again, the experiments were performed for 5 different [KCl] concentrations:

$$\mathrm{c} \in C_{\mathrm{C}} = \{0, 5, 10, 20, 30\} \quad \text{in mM},$$

and for 2 different amplitudes of the electroporation pulse

$$\mathrm{v} \in V = \{12, 30\} \quad \text{in V}.$$

For each couple of $(\mathrm{c}, \mathrm{v}) \in C_{\mathrm{C}} \times V$, experiments were performed in duplicate. The instants after pulse are denoted as

$$\mathrm{t} \in T = \{\mathrm{t}_n = n \times 210 \text{ ms},\ n = 0, 1, \ldots, 1500\}.$$

The measured impedances before (resp. after) the electroporating pulse are denoted by $Z^{(\mathrm{c},\mathrm{v})}_{\mathrm{C,BP},\mathcal{M}}$ (resp. $Z^{(\mathrm{c},\mathrm{v},\mathrm{t})}_{\mathrm{C,AP},\mathcal{M}}$). Figure 4 shows all measurements taken during an experiment with cells, a

[KCl] concentration in the buffer of 5 mM and an electroporation pulse voltage of 12 V. In green one can see the 97 measurements made before the pulse and in blue the 10507 measurements made after the electroporation pulse. The blue color becomes clearer with time. The schematic of Figure 3 illustrates the timing of the experiments. The color (green, navy blue to light blue) of the curve in the upper part of Figure 4 refers to the corresponding experimental phase of the scheme.

2.3 Calibration strategy using buffers data

The measured impedances $Z^{(\mathrm{c})}_{\mathrm{B},\mathcal{M}}$, $Z^{(\mathrm{c,v})}_{\mathrm{C,BP},\mathcal{M}}$ and $Z^{(\mathrm{c,v,t})}_{\mathrm{C,AP},\mathcal{M}}$ differ from the true sample impedances – respectively denoted by $Z^{(\mathrm{c})}_{\mathrm{B},\mathcal{T}}$, $Z^{(\mathrm{c,v})}_{\mathrm{C,BP},\mathcal{T}}$ and $Z^{(\mathrm{c,v,t})}_{\mathrm{C,AP},\mathcal{T}}$ – because of distortion due to the experimental set-up. Following, we present the mathematical strategy to address this problem.

The [KCl] concentration is known for each experiment and the the Kohlrausch law states the link between the conductivity and the [KCl] concentration

$$\sigma(\mathrm{c}) = \sigma_0 + c\Lambda(\mathrm{c}), \quad \text{where} \quad \Lambda(\mathrm{c}) = \Lambda_0 - K\sqrt{\mathrm{c}}, \tag{1}$$

K being the Kohlrausch coefficient – which depends on the stoichiometry of the KCl – and Λ_0 being the molar conductivity at infinite dilution [17]. As previously explained, the buffer conductivity without [KCl] is measured at $\sigma_0 = 0.098$ S.m^{-1}.

The preliminary step consists in optimizing the parameters K and Λ_0 of the [KCl] molar conductivity given in (1). To perform this estimate, we use the data obtained by Vanýsek on [KCl] molar conductivity (see Chapter 5,p 5–92 [10]). The data are not reproduced here for conciseness, but the calibration of Kolrausch's law with the measurements of Vanýsek is given in Figure 11 in Appendix A.

Once this concentration-dependent conductivity is obtained, the buffer at the concentration c of [KCl] (c ranges from 0 to 100 mM) is considered as a solute of conductivity $\sigma(\mathrm{c})$. The theoretical frequency dependent impedance of the buffer denoted by $Z^{(\mathrm{c})}_{\mathrm{B,th}}$ reads then

$$Z^{(\mathrm{c})}_{\mathrm{B,th}}(f) = \frac{k}{\sigma(\mathrm{c})}, \quad \forall f \geq 0. \tag{2}$$

In order to obtain quite comparable values between the measured and true impedance values, we fix $k = 40$ m^{-1}. It is worth noting that the value of k has no influence on the process of calibration since it appears in all the forthcoming impedances.

It is now required to link the theoretical and the measured buffer impedances. Bao *et al.* have shown that the true impedance of the sample $Z_{\mathcal{T}}$ and the measured impedance $Z_{\mathcal{M}}$ are linked nonlinearly through 3 frequency dependent functions A_1, A_2 and A_3:

$$Z_{\mathcal{T}} = \frac{A_1 Z_{\mathcal{M}} + A_2}{Z_{\mathcal{M}} + A_3}. \tag{3}$$

In the set-up of Bao *et al.*, the calibration functions A_1, A_2 and A_3 are not modified when the sample to characterize is changed. In particular, even though the coefficients $A_{1,2,3}$ of Bao *et al.* depend on the buffer, it has no impact on the sample characterization. On the contrary, in our experimental set-up the addition of [KCl] changes both the buffer and the sample, complexifying the calibration. As a first approximation, we consider that the calibration functions $A_{1,2,3}$ of our set-up depend only on the frequency. The quality of the fits (see Figure 6 in Subsection 3.1.2) leads us to believe that this assumption is valid.

Therefore, taking 3 reference samples with known impedances is sufficient to determine these functions at any frequency f, (by simply solving the linear problem satisfied by the calibration

functions $(A_1(f), A_2(f), A_3(f))$). The device of García-Sánchez *et al.* does not exactly fall in this configuration and taking only 3 reference samples leads to unstable calibration. Therefore, to stabilize the calibration procedure, we consider all available measurements without cells at 5 concentrations in duplicate, resulting in 10 references. The estimation is performed through a least squares minimization for overdetermined system. We used the trust-region reflective algorithm (implemented in the function `lsqnonlin` in `Matlab`) to minimize the following cost functions:

$$\mathcal{F}^f_{\mathrm{B}}(A_1(f), A_2(f), A_3(f)) = \sum_{\mathrm{c}\in C_{\mathrm{B}}} \left\| Z^{(\mathrm{c})}_{\mathrm{B,th}}(f) - \frac{A_1(f) Z^{(\mathrm{c})}_{\mathcal{M}}(f) + A_2(f)}{Z^{(\mathrm{c})}_{\mathcal{M}}(f) + A_3(f)} \right\|, \ \forall f \in F_{\mathrm{kHz}}.$$

Once the estimation of $f \mapsto A_1(f)$, $f \mapsto A_2(f)$ and $f \mapsto A_3(f)$ done, it is easy to compute the sample data with cells $Z^{(\mathrm{c,v})}_{\mathrm{C,BP},\mathcal{T}}$ and $Z^{(\mathrm{c,v,t})}_{\mathrm{C,AP},\mathcal{T}}$ by applying formula (3) to $Z^{(\mathrm{c,v})}_{\mathrm{C,BP},\mathcal{M}}$ and $Z^{(\mathrm{c,v,t})}_{\mathrm{C,AP},\mathcal{M}}$.

2.4 Equivalent electric circuit of the experiments

Our strategy to study the impact of electroporation on the electrical properties of the cells consists in analyzing impedance data using an equivalent electrical model of the experimental set-up. Figure 5, Bottom-Right presents the circuit which is composed of two parallel branches, one for the buffer compartment the other one for the cell compartment. An important feature of the set-up lies in the fact that the volume occupied by the cells is not negligible compared with the total volume. Another important –and hardly measurable– phenomenon lies in the ion exchanges between the cells and the buffer. This phenomena is particularly important at low buffer conductivity. Therefore the buffer impedances obtained by the calibration are modified –and thus need to be estimated– in the experiments with cells.

Denoting by $\sigma_{0,b}$ the buffer conductivity without [KCl], the buffer conductivity as a function of the [KCl] concentration is deduced from the Kohlrausch law:

$$\sigma_b([\mathrm{KCl}]_b) = \sigma_{0,b} + [\mathrm{KCl}]_b(\Lambda_0 - K\sqrt{[\mathrm{KCl}]_b}).$$

To account for the cells-buffer ion exchange, we set

$$\sigma_{0,b} = \sigma_0 + \Delta\sigma_0,$$

where $\Delta\sigma_0$ is the change of conductivity due to ions exchange between cells and the buffer that has to be fit. The buffer resistance is then modeled as

$$R^{\mathrm{r}}_b = \frac{R_b}{\phi} = \frac{k}{\sigma_b([\mathrm{KCl}]_b)\phi}, \text{ with } k = 40\mathrm{m}^{-1},$$

where $1-\phi$ is the volume fraction of the cells.

The influence of the cells on the measured impedance is mainly due to the cytoplasm and the membrane of the cells similarly to [5]. The cytoplasm compartment is assumed only conductive while the membranes compartment is modeled by a constant phase element (CPE) of parameters (C_m, α_m) in parallel with a resistance denoted by R_m following [11, Chapter 3]. Before the pulse, R_m is fixed at the value

$$R_m = \frac{k}{(1-\phi)^{2/3} S_m/A_m} = 2.34\ \mathrm{M\Omega},$$

where $A_m = 2 \times 10^4\ \mathrm{m}^{-1}$ is a constant denoting the ratio of membrane area per unit volume and $S_m = 1\ \mathrm{S.m}^{-2}$ is the conductance of the cell membranes per surface unit [23, 9].

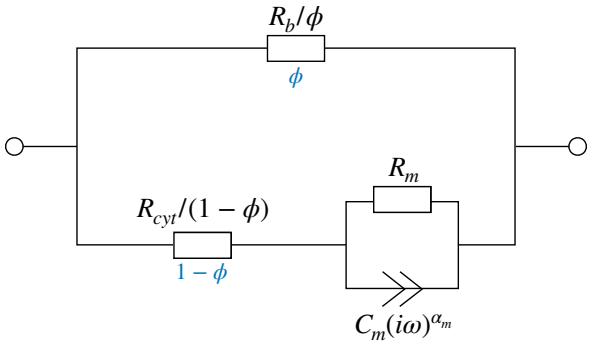

Figure 5: Electrical circuit for the buffer-cells system.

Note that since the experimental set-up is very thin (the height is about 15μm), it is necessary to account for the cell volume fraction denoted here by $1-\phi$. However it is worth noting that if the volume fraction behaves like $1-\phi$ then the membranes compartment behaves like $(1-\phi)^{2/3}$, if the cells are rounded enough. This is the reason why we introduce the parameter $(1-\phi)^{2/3}$ in the membrane resistance R_m.

2.4.1 Cost function and minimization algorithm for the calibration

The impedance of our equivalent circuit with cells $Z_{\mathrm{C,th}}$ (before and after pulse) is defined by

$$\frac{1}{Z_{\mathrm{C,th}}(f,\theta)} = \frac{\sigma_b([\mathrm{KCl}]_b)\phi}{k} + \frac{1}{\dfrac{R_{cyt}}{(1-\phi)} + \dfrac{R_m}{(1+R_m C_m(2i\pi f)^{\alpha_m})}}, \tag{4}$$

where θ is a vector which concatenates the 6 parameters

$$\theta = (\phi, \Delta\sigma_0, [\mathrm{KCl}]_b, R_{\mathrm{cyt}}, \alpha_m, C_m) \in \mathbb{R}^6.$$

Before pulse, the parameters are estimated under the following constraints:

- $\phi \in [0.75; 0.85]$,
- $\Delta\sigma_0 \in [0; 0.5]$ S/m,
- $[\mathrm{KCl}]_b \in [0.95\, c_{th}; 1.05\, c_{th}]$ with $c_{th} = [5, 10, 20, 30]$ mM,
- $R_{\mathrm{cyt}} \in [10; 60]$ Ω,
- $\alpha_m \in [0.8; 1]$,
- $C_m \in [10^{-11}; 10^{-5}]$ F.

Ideally, the parameter ranges should be as large as possible to minimize their influences on the calibration. However, to minimize computational costs and control uncertainties arising from the model and the data, and because the model parameters are not necessarily identifiable without constraints, we restrict the parameters to the above ranges, which seems reasonably restrictive.

Moreover, R_m is fixed at the value 2.34 MΩ described above. Indeed, large variations of R_m result in a similar fit (numerical tests not shown), indicating that R_m is not identifiable. Fixing the value of R_m stabilizes the calibration.

After pulse, the parameters are fixed at the estimated values before pulse except R_m and $[\mathrm{KCl}]_b$ which are fit by the minimization algorithm without any model. In particular, we decide to omit the change in R_{cyt} after the pulse as well as ϕ, which represents cell swelling. Swelling was not observed after the pulse, at least not in a significant way. This is not surprising because the sucrose content of the extracellular buffer was adjusted to make it isosmotic and avoid cell swelling. Moreover from a mathematical point of view, considering R_{cyt} and ϕ as additional parameters makes the system unidentifiable. Keeping R_{cyt} constant and $[\mathrm{KCl}]_b$ as a variable parameters is somehow equivalent to consider that the changes of [KCl] concentration has the most impact on the total impedance. This is justified by the fact that the cell concentration of [KCl] is about 140 mM, while the outer concentration before the pulse ranges from 0 to 30 mM.

The estimation of the parameters is performed using the trust-region reflective algorithm (implemented in the function `lsqnonlin` in `Matlab`) to minimize the following relative cost functions

$$\mathcal{F}_{\mathrm{BP}}^{(\mathrm{c,v})}(\theta) = \frac{1}{|F|} \sum_{f \in F_{\mathrm{kHz}}} \frac{|Z_{\mathrm{C,th}}(f,\theta) - Z_{\mathrm{C,BP},\mathcal{T}}^{(\mathrm{c,v})}(f)|}{|Z_{\mathrm{C,BP},\mathcal{T}}^{(\mathrm{c,v})}(f)|}, \forall \mathrm{c} \in C_{\mathrm{C}}, \forall \mathrm{v} \in V, \tag{5a}$$

$$\mathcal{F}_{\mathrm{AP}}^{(\mathrm{c,v,t})}(\theta) = \frac{1}{|F|} \sum_{f \in F_{\mathrm{kHz}}} \frac{|Z_{\mathrm{C,th}}(f,\theta) - Z_{\mathrm{C,AP},\mathcal{T}}^{(\mathrm{c,v,t})}(f)|}{|Z_{\mathrm{C,AP},\mathcal{T}}^{(\mathrm{c,v,t})}(f)|}, \forall \mathrm{c} \in C_{\mathrm{C}}, \forall \mathrm{v} \in V, \forall \mathrm{t} \in T. \tag{5b}$$

The quality of the fits is evaluated by computing the values of $\mathcal{F}_{\mathrm{BP}}^{(\mathrm{c,v})}(\theta_{\mathrm{e}})$ and $\mathcal{F}_{\mathrm{AP}}^{(\mathrm{c,v,t})}(\theta_{\mathrm{e}})$ where θ_{e} is the vector of estimated parameters.

3 Results

3.1 Set-up calibration

3.1.1 Kohlrausch parameters estimation

The preliminary step is to obtain the Kohlrausch parameters in order to link the [KCl] concentration to the conductivity of the buffer. The best value of K and Λ_0 that fits – see Figure 11 in Appendix A – the law (1) are $K = 7.17$ SI and $\Lambda_0 = 14.98$ SI.

3.1.2 Calibration functions A_1, A_2, A_3

As explained in the previous section, the calibration of the set-up consists in finding the frequency-dependent function A_1, A_2, A_3 to link the sample (buffer without cells) impedance to the measurements by the equality (3). The estimated functions A_1, A_2 and A_3 are given in Figure 6a (solid lines). The dashed lines correspond to the calibration method proposed by Bao *et al.* –using only 3 dataset among the 5– while the thick solid lines correspond to our method with the whole dataset. One can see that the calibration of Bao *et al.* is unstable for the set-up of García *et al.*, while our calibration seems more robust.

The interesting fact is that these calibration functions A_1, A_2, A_3 enable to obtain relevant buffer impedance. Indeed, as seen in Figure 6b, the calibrated data without cells obtained from (3) shows that the buffer behaves like a conductive solute.

In addition, Figure 6b shows that the theoretical sample impedances obtained with the model (2) (solid lines) are in very good accordance with the sample impedance obtained after calibration with (3) (circle markers).

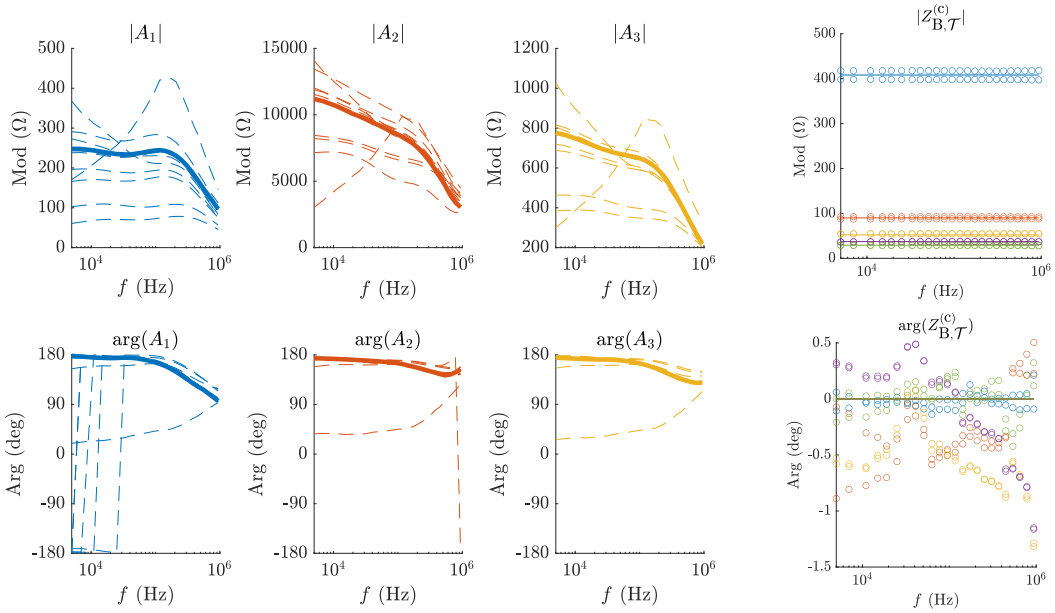

Figure 6: (a): Estimations of the functions A_1, A_2 and A_3 for all possible configurations in dashed lines and estimations using all the available data in solid lines. (b): Calibrated sample impedances without cells $Z^{(c)}_{B,\mathcal{T}} = \frac{A_1 Z^{(c)}_{B,\mathcal{M}} + A_2}{Z^{(c)}_{B,\mathcal{M}} + A_3}$ (circle markers) compared with theoretical impedances $Z^{(c)}_{B,th}$ (lines).

3.2 Calibration of the equivalent circuit before and after the pulse delivery

The true impedances of the samples with cells before $Z^{(\mathrm{c,v})}_{\mathrm{C,BP},\mathcal{T}}$ and after $Z^{(\mathrm{c,v})}_{\mathrm{C,AP},\mathcal{T}}$ are obtained from the measurements before and after the pulse respectively by using the above calibration functions:

$$Z^{(\mathrm{c,v})}_{\mathrm{C,BP},\mathcal{T}} = \frac{A_1 Z^{(\mathrm{c,v})}_{\mathrm{C,BP},\mathcal{M}} + A_2}{Z^{(\mathrm{c,v})}_{\mathrm{C,BP},\mathcal{M}} + A_3} \quad \text{and} \quad Z^{(\mathrm{c,v,t})}_{\mathrm{C,AP},\mathcal{T}} = \frac{A_1 Z^{(\mathrm{c,v,t})}_{\mathrm{C,AP},\mathcal{M}} + A_2}{Z^{(\mathrm{c,v,t})}_{\mathrm{C,AP},\mathcal{M}} + A_3},$$

for any triple $\{\mathrm{c,v,t}\} \in C_{\mathrm{C}} \times V \times T$. The parameters of the model are given by Table 1. Interestingly, one sees that the parameter $\Delta\sigma_0$ varies between different experiments. This is probably due the variability of the release of ions in the buffer by the cells.

	12 V				30 V			
[KCl] concentration (mM)	5	10	20	30	5	10	20	30
vol. frac. ϕ - exp1	0.79	0.82	0.81	0.85	0.83	0.84	0.85	0.85
vol. frac. ϕ - exp2	0.76	0.84	0.85	0.85	0.8	0.85	0.85	0.84
$\Delta\sigma_0$ (S/m) - exp1	8.3×10^{-6}	1.6×10^{-4}	0.097	0.5	0.15	0.12	0.27	0.2
$\Delta\sigma_0$ (S/m) - exp2	0	0.13	0.37	0.26	0.0016	0.2	0.26	0.44
$[\mathrm{KCl}]_b$ (mM) - exp1	4.8	9.6	19.9	29.4	4.9	9.9	20	29.4
$[\mathrm{KCl}]_b$ (mM) - exp2	4.8	10	20	30	4.8	10	20.1	30.5
$R_{\mathrm{cyt}}/(1-\phi)$ (Ω) - exp1	265	276	260	372	275	340	359	372
$R_{\mathrm{cyt}}/(1-\phi)$ (Ω) - exp2	238	285	375	349	256	375	369	311
α_m - exp1	0.85	0.86	0.83	0.81	0.83	0.89	0.83	0.8
α_m - exp2	0.84	0.85	0.81	0.82	0.82	0.9	0.83	0.8
C_m (nF) - exp1	17.4	14.9	20.8	6.13	18.1	8.09	9.62	15.5
C_m (nF) - exp2	24	13.8	13.8	5.96	28.1	6.13	11.1	14.8
$\frac{1}{\lvert T\rvert}\sum_{\mathrm{t}\in T}\mathcal{F}^{(\mathrm{c,v,t})}_{\mathrm{AP}}(\theta_{\mathrm{e}})$ - exp1	0.015	0.01	0.009	0.009	0.0082	0.0078	0.0062	0.0065
$\frac{1}{\lvert T\rvert}\sum_{\mathrm{t}\in T}\mathcal{F}^{(\mathrm{c,v,t})}_{\mathrm{AP}}(\theta_{\mathrm{e}})$ - exp2	0.015	0.011	0.01	0.0073	0.012	0.0068	0.0062	0.011

Table 1: Estimated parameters of the equivalent circuit given in Figure 5 before pulse. R_m is set to 2.34 MΩ for the 2 experiments (exp1 and exp2).

The resulting Bode plots are given in Figure 7 where dot markers shows the calibrated data with cells for $\mathrm{t} \in \{0, 30, \cdots, 300\}$ s for experimental set-up at v = 12 V. As expected, the generated true impedances with cells before the pulse delivery $Z^{(\mathrm{c,v})}_{\mathrm{C,BP},\mathcal{T}}$ display a flat modulus for low frequencies. This is due to the shielding effect of the membrane at low frequency. These results validate simultaneously our calibration procedure and the electrical circuit combined with Kohlrausch's conductivity to model the buffer. The curves with v = 30 V are given in Appendix C. One can seen again that the impedances are accurately determined by the model. The errors on the phase are smaller than 2 degrees (for 12 V and 30 V) and the relative errors on the amplitudes are smaller that 1% for 12 V and for 30 V, which is very satisfactory for such a complex experimental set-up.

3.3 Evolution of the membrane compartment resistance and the buffer conductivity immediately after the pulse

The previous calibration enables us to follow the influence of electroporation on the changes in the parameters corresponding to the cell membrane of the equivalent electrical circuit proposed. Figure 8 presents the evolution of R_m and of the [KCl] concentration during 2 seconds after electroporation. Let us emphasize that this postpulse calibration of R_m and $[\mathrm{KCl}]_b$ is performed without any *a priori* on the evolution of these 2 parameters.

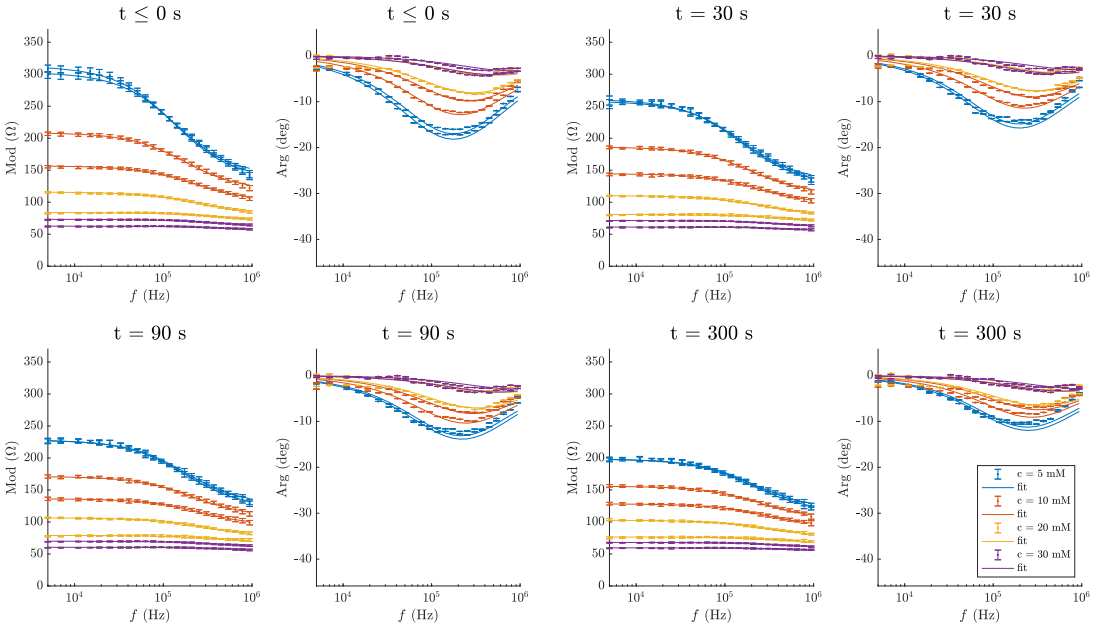

Figure 7: Bode plot of $Z^{(\mathrm{c},12)}_{\mathrm{C,BP},\mathcal{T}}$ (top-left) and $Z^{(\mathrm{c},12,\mathrm{t})}_{\mathrm{C,AP},\mathcal{T}}$ at different times for $\mathrm{c} \in C$.

Within the first milliseconds after the pulse, the dynamics of the membrane resistance R_m exhibits a very fast and large decrease due to the pulse followed by a small increase (see Figure 8). This first dynamic on the membrane, could be interpreted as the opening and closing pores of the membrane due to the pulse. An interesting point is that the membrane resistance immediate drop is much higher at 30 V than at 12 V (see Figure 8) which is here again consistent with the classical view of electropermeabilisation (the pulses with larger magnitude create more defects that the pulse at low magnitude).

4 Discussion

We propose in this paper a well-designed calibration procedure and an equivalent electric circuit model for the 4-electrode experimental set-up of García-Sánchez *et al.* It is worth noting that bioimpedancemetry is a powerful but complex methodology to track the properties of living tissues or cell aggregates [24]. One can cite the recent review of Abasi *et al.* [1]. Here the difficulty is even higher because the electric field generates defects in cell membrane, leading to ions exchanges between cells and the buffer. This phenomenon complexifies the interpretation of the bioimpedancemetry.

Our numerical strategy enables us to decipher the electrical dynamics of the cell membrane compartment within the first seconds after the pulse.

4.1 Huge variability of the calibration functions using only 3 data without cells

First the calibration strategy of Bao *et al.* using only 3 data sets to obtain the calibration functions A_1, A_2, A_3 was not stable. Indeed, one can remark that these functions strongly depend on the choice of the 3 data sets. To overcome the instability, we use all the available data and performed the calibration with a nonlinear optimization procedure. As shown by Figure 6a, our procedure is more robust.

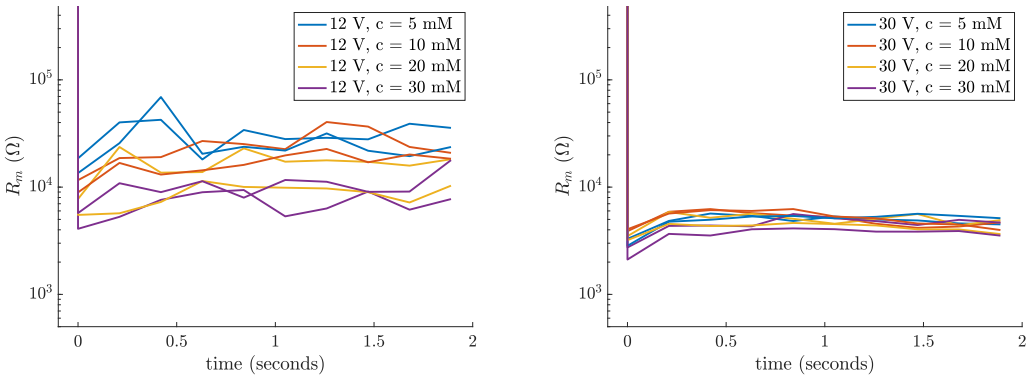

(a) Exp. pulse at 12V

(b) Exp. pulse at 30V

Figure 8: Evolutions of the membrane resistance R_m within the first 2 seconds after the permeabilizing pulse (12V and 30V resp.).

4.2 Data variability between two same experiments

One can remark the data variability between two same experiments, as for example for c = 10 or 20 mM with v = 12 V (see Figure 7) or for c = 5 mM with v = 30 V (see Figure 13). We assume that this variability is due to different states of the cells and exchanges between the cell monolayer and the buffer. The parameter $\Delta\sigma_0$ has been added to the buffer conductivity in order to account for this phenomenon.

4.3 Discriminating buffer conductivity increase and membrane permeabilisation

Experiment	v (V)	c (mM)	$[KCl]_b^{begin}$	$[KCl]_b^{end}$	$\tau_{[KCl]_b}$
1	12	5	5.17	9.29	98.9
2	12	5	5.15	9.65	91.2
1	12	10	9.92	13.5	86.8
2	12	10	11.2	14.3	71.3
1	12	20	20.9	22.9	64.6
2	12	20	22.6	25.7	103
1	12	30	33	35.2	79.6
2	12	30	32.2	34.5	101
1	30	5	6.84	13.8	38.4
2	30	5	5.94	13.2	36.3
1	30	10	11.7	18.1	34.6
2	30	10	12.3	18.4	42.4
1	30	20	22.8	28	45.9
2	30	20	22.5	27.5	42.4
1	30	30	31.3	35.5	43.1
2	30	30	34	37.7	34.8

Table 2: Values obtained when fitting the $[KCl]_b$ concentration with the function given in Equation (6).

4.3.1 Deriving a model on the [KCl] concentration

The calibration after the pulse was performed without any a priori, meaning without any model neither on [KCl] nor on R_m. However it could be interesting to derive a model on the [KCl] concentration evolution to decrease the cost of computation of the calibration and to extract the time constant of the release of [KCl] after the pulse. Previous studies linked similar post-field conductivity dynamics to exponential models of transport of ions through the membrane (see Fig. 6 and equation (2) of [19]). Other studies using ultrashort pulses and small molecules such as YO-PRO1 also described very similar dynamics to the ones provided by our model to [KCl]. One refers for example to [22]. Therefore, the evolutions of the [KCl] concentrations after the pulse can be described by following the function (Figure 14 given in the appendix section D)

$$[\mathrm{KCl}]_b^{\mathrm{fit}} = [\mathrm{KCl}]_b^{\mathrm{begin}} + ([\mathrm{KCl}]_b^{\mathrm{end}} - [\mathrm{KCl}]_b^{\mathrm{begin}})(1 - e^{-t/\tau_{[\mathrm{KCl}]_b}}), \tag{6}$$

for which only 3 parameters have to be fitted for each experiment instead of the calibration of the 10507 timepoints. Table 2 contains the estimated values of these 3 parameters for each experiment. From Table 2 one sees that for a given experiment, the release of [KCl] –that is $[\mathrm{KCl}]_b^{\mathrm{end}} - [\mathrm{KCl}]_b^{\mathrm{begin}}$– is higher after the pulse at 30 V than at 12 V, and the time constant of the release $\tau_{[\mathrm{KCl}]_b}$ is shorter at 30 V than at 12 V, meaning the dynamics of the release is faster at 30 V than at 12 V. Another interesting observation is the fact that the time constants $\tau_{[\mathrm{KCl}]_b}$ are similar between all the experiments for a given voltage, which is consistent with the fact that the permeabilisation depends on the magnitude of the pulse. We eventually note that for higher initial concentration in the buffer, the release is smaller due to a lower gradient between the cell and the buffer [KCl] concentrations.

4.3.2 How to track the long-term behaviour of the membranes?

Regarding the evolution of the membrane resistance, the calibration shows that the membrane compartment does not recover its initial resistance after 5 minutes to its value before the pulse, as shown on Figure 9.

Even though there are several experimental observations that electroporation lasts several minutes [18, 13], it is unlikely that the membrane resistance keeps decreasing after several tens of seconds. It is difficult to say whether this behavior of our estimated membrane resistance R_m is due to measurement errors leading to overfitting, or to the simplicity of our equivalent circuit, or to both. Future work consisting of performing a 3D simulation – corresponding to a more complex model than the equivalent circuit – of the entire experimental setup could shed light on the model. As for the overfitting, we perform a numerical simulation assuming that the membrane resistance increases after the pulse. All estimated membrane resistances are shown in Figure 10-Top-Left for v = 12V. The corresponding impedance fits are shown in Figure 10-Right for v = 12V and for 3 different times. Interestingly, one can see that the fits are not degraded that much, which would be consistant with an overfitting. It is important to emphasize that the estimates of the conductivity $[\mathrm{KCl}]_b$ are very close to the previously estimated conductivities, see Figure 10-Bottom-Left. Maybe that a few time-point measurements of the buffer conductivity after the pulse to validate the estimates of the $[\mathrm{KCl}]_b$ concentration would make it possible to track the long-time behaviour of the membrane after the pulse. We think that some time point measurements of buffer conductivity after the pulse may or may not confirm the very stable estimates of $[\mathrm{KCl}]_b$ concentration. This could correct possible errors in the estimates and better track the long-term behaviour of the membrane after the pulse, even if this results in a degradation of the fit quality.

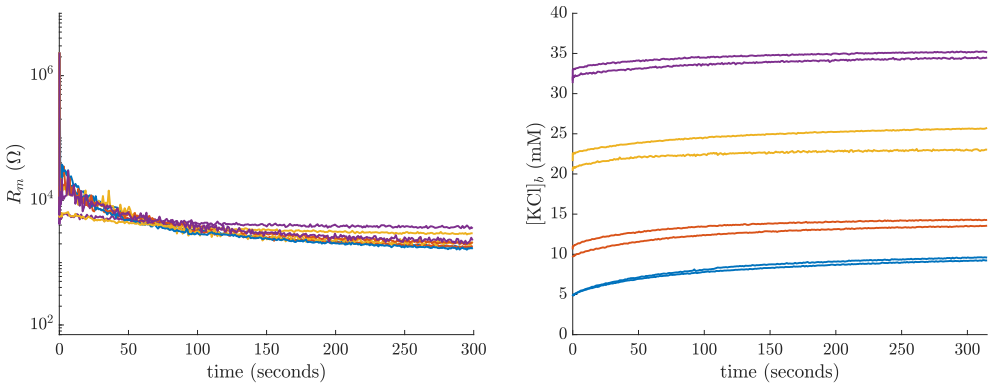

(a) Exp. pulse at 12V

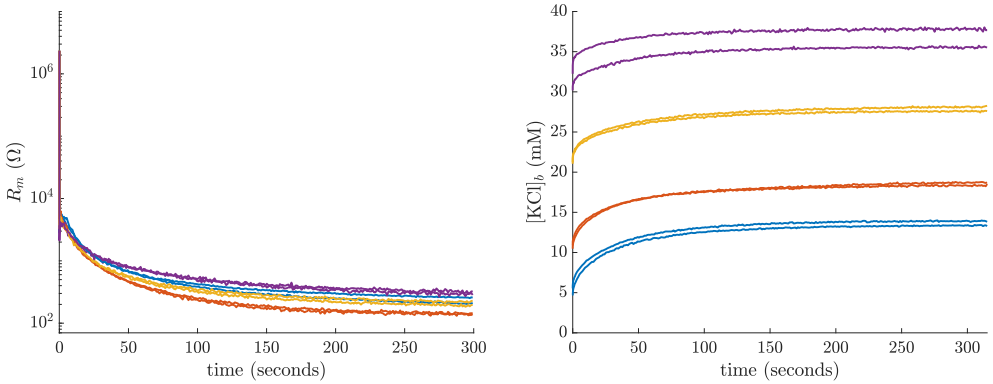

(b) Exp. pulse at 30V

Figure 9: Time evolutions of the membrane resistance R_m (first column) and [KCl] concentration.

5 Conclusion and perspectives

We proposed in this paper a well-designed numerical procedure to exploit data sets obtained by the complex 4-electrode experimental set-up of García-Sánchez *et al.* to track post pulse membrane behaviors.

Thanks to a robust calibration procedure of the set-up, the data sets without and with cells were exploited successively to calibrate appropriately the electrical circuit equivalent to the set-up. The interesting point is that we were able to discriminate between the release of [KCl] and the membrane resistance dynamics within the first seconds after the pulse. Our calibration suggest that to track the membrane dynamics during the 5 min after the pulse, additional measurements of the buffer conductivity should be performed, for example at the end of the experiment.

Another strategy for tracking membrane dynamics during the 5 minutes after the pulse is to consider a more complex mathematical model. It seems that nothing justifies a more complex circuit model. Although we are convinced that our equivalent electric circuit approach was a necessary step before increasing the complexity of the numerical strategy, it does reveal some limitations. Therefore, we would like to perform a 3D simulation of the whole experimental set-up.

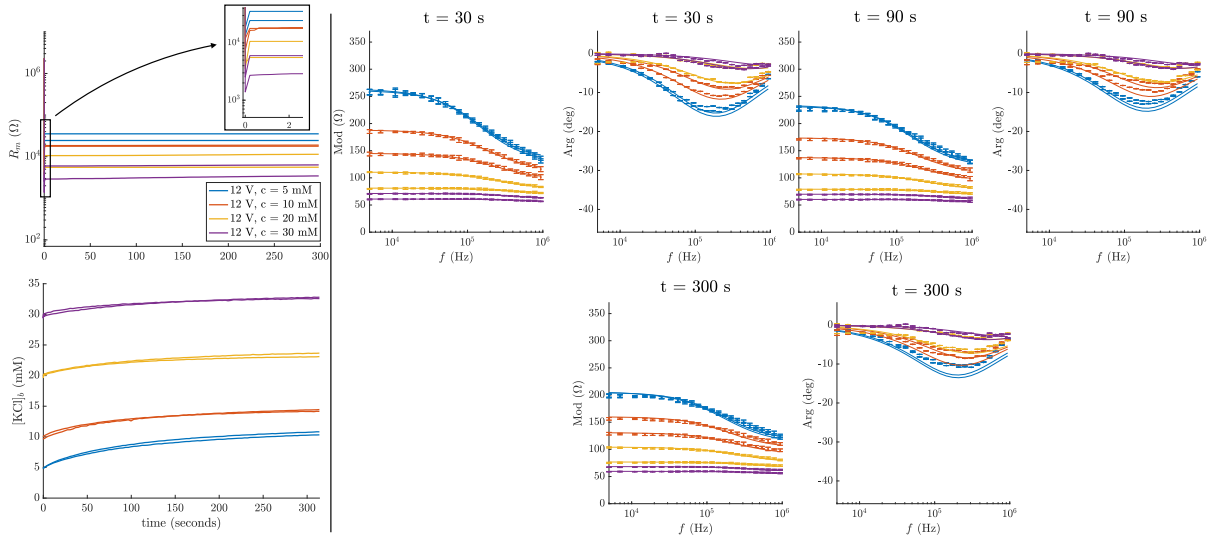

Figure 10: Left-Top: Time evolutions of the membrane resistance R_m when we impose its increasing. Left-Right: Time evolutions of the $[\mathrm{KCl}]_b$ concentration when we impose the increasing of R_m. Right: Corresponding bode plot of $Z^{(\mathrm{c},12,\mathrm{t})}_{\mathrm{C,AP},\mathcal{T}}$ at 3 times for $\mathrm{c} \in C$.

References

[1] S. Abasi, J. R. Aggas, G. G. Garayar-Leyva, B. K. Walther, and A. Guiseppi-Elie. Bioelectrical impedance spectroscopy for monitoring mammalian cells and tissues under different frequency domains: A review. ACS Measurement Science Au, 2(6):495–516, 2022.

[2] J.-Z. Bao, C. C. Davis, and R. E. Schmukler. Impedance spectroscopy of human erythrocytes: system calibration, and nonlinear modeling. IEEE Transactions on biomedical engineering, 40(4):364–378, 1993.

[3] M. Breton, L. Delemotte, A. Silve, L. M. Mir, and M. Tarek. Transport of sirna through lipid membranes driven by nanosecond electric pulses: An experimental and computational study. Journal of the American Chemical Society, 134(34):13938–13941, 2012. PMID: 22880891.

[4] R. V. Davalos, L. Mir, and B. Rubinsky. Tissue ablation with irreversible electroporation. Annals of biomedical engineering, 33(2):223, 2005.

[5] E. Fear and M. Stuchly. Modeling assemblies of biological cells exposed to electric fields. IEEE Transactions on Biomedical Engineering, 45(10):1259–1271, 1998.

[6] T. García-Sánchez, A. Azan, I. Leray, J. Rosell-Ferrer, R. Bragos, and L. M. Mir. Interpulse multifrequency electrical impedance measurements during electroporation of adherent differentiated myotubes. Bioelectrochemistry, 105:123–135, 2015.

[7] J. Gehl. Electroporation for drug and gene delivery in the clinic: doctors go electric. Electroporation Protocols, pages 351–359, 2008.

[8] P. B. Ishai, M. S. Talary, A. Caduff, E. Levy, and Y. Feldman. Electrode polarization in dielectric measurements: a review. Measurement Science and Technology, 24(10):102001, 2013.

[9] O. Kavian, M. Leguèbe, C. Poignard, and L. Weynans. "classical" electropermeabilization modeling at the cell scale. Journal of Mathematical Biology, 68(1):235–265, Jan 2014.

[10] D. R. Lide et al. Crc handbook of chemistry and physics, 84th. Electrochemical Series. CRC Press LLC, 2004.

[11] V. F. Lvovich. Impedance spectroscopy: applications to electrochemical and dielectric phenomena. John Wiley & Sons, 2012.

[12] F. M Andre and L. M Mir. Nucleic acids electrotransfer in vivo: mechanisms and practical aspects. Current gene therapy, 10(4):267–280, 2010.

[13] C. Merla, M. Nardoni, M. Scherman, S. Petralito, L. Caramazza, F. Apollonio, M. Liberti, P. Paolicelli, B. Attal-Tretout, and L. M. Mir. Changes in hydration of liposome membranes exposed to nanosecond electric pulses detected by wide-field coherent anti-stokes raman microspectroscopy. Bioelectrochemistry, 147:108218, 2022.

[14] D. Miklavčič, G. Serša, E. Brecelj, J. Gehl, D. Soden, G. Bianchi, P. Ruggieri, C. R. Rossi, L. Campana, and T. Jarm. Electrochemotherapy: technological advancements for efficient electroporation-based treatment of internal tumors. Medical & biological engineering & computing, 50(12):1213–1225, 2012.

[15] L. M. Mir. Therapeutic perspectives of in vivo cell electropermeabilization. Bioelectrochemistry, 53(1):1–10, 2001.

[16] L. M. Mir, S. Orlowski, J. Belehradek, and C. Paoletti. Electrochemotherapy potentiation of antitumour effect of bleomycin by local electric pulses. European Journal of Cancer and Clinical Oncology, 27(1):68 – 72, 1991.

[17] T. Murphy and E. Cohen. Corrections to the fuoss–onsager theory of electrolytes. The Journal of Chemical Physics, 53(6):2173–2186, 1970.

[18] A. G. Pakhomov, J. F. Kolb, J. A. White, R. P. Joshi, S. Xiao, and K. H. Schoenbach. Long-lasting plasma membrane permeabilization in mammalian cells by nanosecond pulsed electric field (nspef). Bioelectromagnetics, 28(8):655–663, 2007.

[19] M. Schmeer, T. Seipp, U. Pliquett, S. Kakorin, and E. Neumann. Mechanism for the conductivity changes caused by membrane electroporation of CHO cell-pellets. Physical Chemistry Chemical Physics, 6(24):5564, 2004.

[20] H. Schwan. Alternating current electrode polarization. Biophysik, 3(2):181–201, 1966.

[21] H. P. Schwan and C. D. Ferris. Four-electrode null techniques for impedance measurement with high resolution. Review of scientific instruments, 39(4):481–485, 1968.

[22] E. B. Sözer, Z. A. Levine, and P. T. Vernier. Quantitative limits on small molecule transport via the electropermeome — measuring and modeling single nanosecond perturbations. Scientific Reports, 7(1), Mar. 2017.

[23] J. Teissie, M. Golzio, and M. Rols. Mechanisms of cell membrane electropermeabilization: a minireview of our present (lack of?) knowledge. Biochimica et Biophysica Acta (BBA)-General Subjects, 1724(3):270–280, 2005.

[24] Y. D. Yalcin and R. Luttge. Electrical monitoring approaches in 3-dimensional cell culture systems: Toward label-free, high spatiotemporal resolution, and high-content data collection in vitro. Organs-on-a-Chip, 3:100006, 2021.

Supplementary Materials

A Kohlrausch parameters estimation

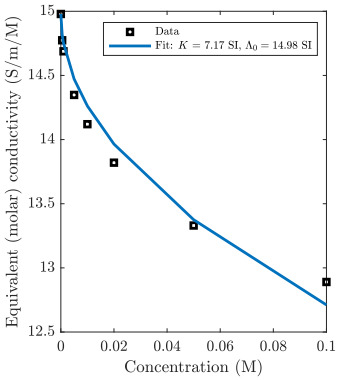

Figure 11: Calibration of Kohlrausch law with the data of Vanýsek [10] (Chapter 5, p. 5-92). The continuous line is the Kohlrausch law with $K = 7.17$ SI and $\Lambda_0 = 14.98$ SI.

B Calibrated data for v = 30 V

Figure 12 shows the measured and the calibrated impedances before pulse for each concentration at voltage v = 30 V.

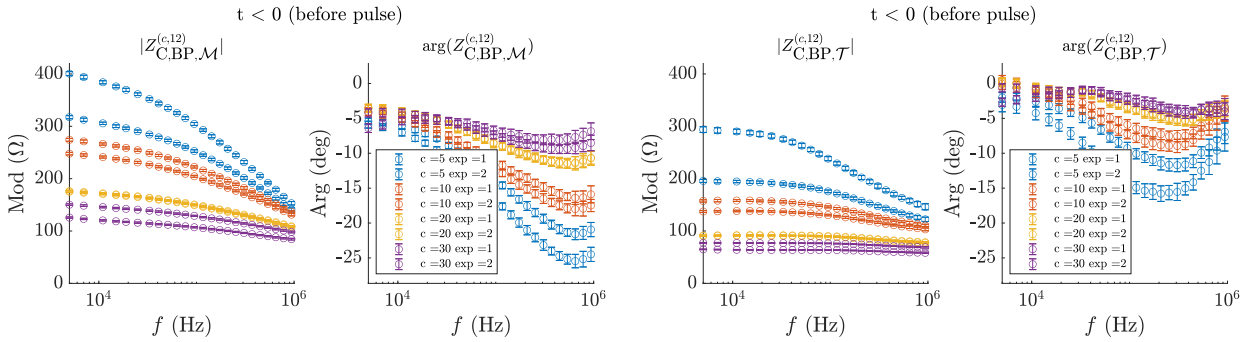

Figure 12: Left: measured impedances $Z^{(c,30)}_{C,BP,\mathcal{M}}$ before pulse for each concentration at voltage v = 30 V. Right: calibrated impedances $Z^{(c,30)}_{C,BP,\mathcal{T}}$ before pulse for each concentration at voltage v = 30 V

C Supplementary figures of the calibration with the equivalent circuit

Figure 13 (dot markers) shows the calibrated data with cells for t $\in \{0, 30, \cdots, 300\}$ s and for v = 30 V.

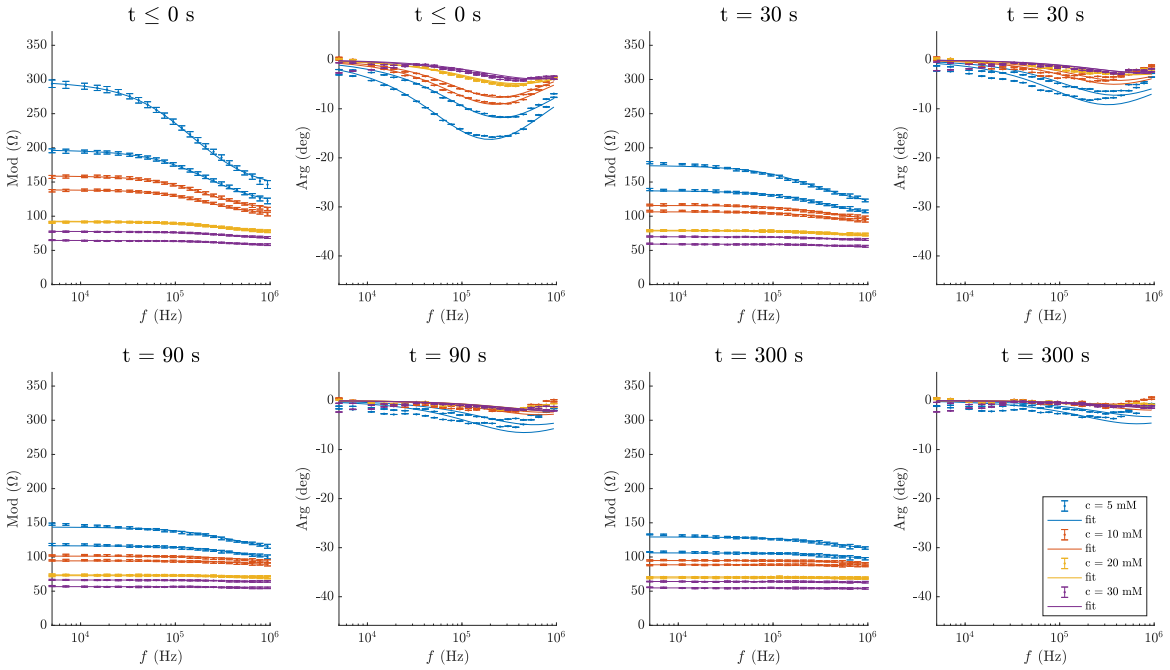

Figure 13: Calibrated sample impedances $Z^{(c,30)}_{C,BP,\mathcal{T}}$ (top-left) and $Z^{(c,30,t)}_{C,AP,\mathcal{T}}$ for $t \in \{0, 30, \cdots, 300\}$ s and for $c \in C$.

D Comparisons of the calibration and the 3-parameter model for the [KCl] concentrations

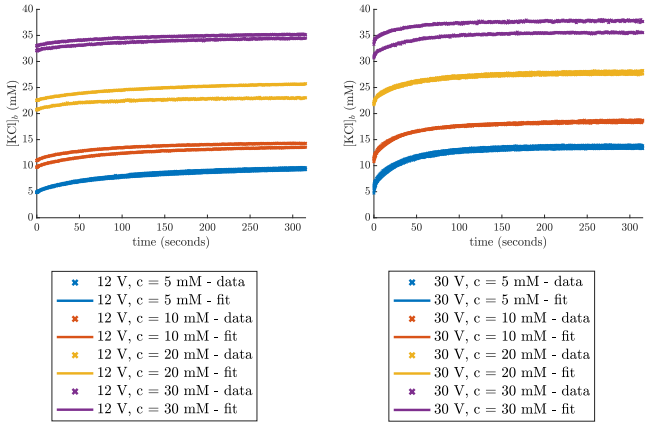

Figure 14: $[KCl]_b$ concentrations and fits obtained when fitting them with the function given in Equation (6).